PCCP

Accepted Manuscript

ROYAL SOCIETY OF CHEMISTRY

www.rsc.org/pccp

PCCP

RSCPublishing

ARTICLE

Optimization of thermoelectric efficiency in SnTe: The case for the light band

Cite this: DOI: 10.1039/xoxxoooooox

Received ooth January 2012,
Accepted ooth January 2012

DOI: 10.1039/xoxxoooooox

www.rsc.org/

Min Zhou[1, 3,†], Zachary M. Gibbs[2,†], Heng Wang[3], Yemao Han[1], Caini Xin[1], Laifeng Li[1,*], G. Jeffrey Snyder[3,4,*]

[1] Key Laboratory of Cryogenics, Technical Institute of Physics and Chemistry, Chinese Academy of Sciences, Beijing 100190, China
[2] Division of Chemistry and Chemical Engineering, California Institute of Technology, 1200 E. California Blvd. Pasadena, CA 91125, USA
[3] Materials Science, California Institute of Technology, 1200 California Blvd., Pasadena, CA 91125, USA
[4] ITMO University, Saint Petersburg Russia

P-type PbTe is an outstanding high temperature thermoelectric material with zT of 2 at high temperatures due to its complex band structure which leads to high valley degeneracy. Lead-free SnTe has a similar electronic band structure, which suggests that it may also be a good thermoelectric material. However, stoichiometric SnTe is a strongly p-type semiconductor with a carrier concentration of about 1×10^{20} cm^{-3}, which corresponds to a minimum Seebeck coefficient and zT. While in the case of p-PbTe (and n-type La_3Te_4) one would normally achieve higher zT by doping into the deeper band with higher valley degeneracy, SnTe behaves differently. It is the lighter, upper valence band is shown in this work to result in a higher zT. Therefore decreasing the hole concentration to maximize performance of the light band results in higher zT than doping into the high degeneracy heavy band. Here we tune the electrical transport properties of SnTe by decreasing carrier concentration with Iodine doping, and increasing the carrier concentration with Gd or Te doping. A peak zT value of 0.6 at 700 K was obtained for $SnTe_{0.985}I_{0.015}$ which optimizes the light, upper valence band, which is about 50% higher than the other peak zT value of 0.4 for $Gd_zSn_{1-z}Te$ and $SnTe_{1+y}$ which optimize the high valley degeneracy lower valence band.

---

† Min Zhou and Zachary M. Gibbs have contributed equally to this work.

* Prof. Laifeng Li, Key Laboratory of Cryogenics, Technical Institute of Physics and Chemistry, Chinese Academy of Sciences, Beijing 100190, China. E-mail: laifengli@mail.ipc.ac.cn
* Dr. G. Jeffrey Snyder, Materials Science, California Institute of Technology, Pasadena, CA 91125, USA. E-mail: jsnyder@caltech.edu

PCCP

RSCPublishing

ARTICLE

1. Introduction

Supplying and maintaining a clean energy supply is an increasingly important goal. Waste heat recovery using thermoelectric materials is one pathway towards this end, but conversion efficiency in these materials is still quite low. The figure of merit, $zT=\alpha^2T/\rho(\kappa_e+\kappa_L)$, determines the conversion efficiency where α is the Seebeck coefficient, T is the temperature, ρ is the electronic resistivity, κ_e and κ_L are electronic and lattice contribution to thermal conductivity. Lead chalcogenides, which have the rock salt structure, are some of the most studied thermoelectric materials and have a record high figure of merit (zT) between 1.4 and 2.2[1-3]. One mechanism of p-type PbTe's outstanding thermoelectric performance is thought to be due to its complex valence band structure, especially at high temperatures where the energy of primary and secondary maximums are thought to be aligned—leading to extraordinarily high valley degeneracy[4].

In SnTe, one might also expect good thermoelectric performance because it shares many of the same characteristics with PbTe; specifically: both exist in the rock salt crystal structure and both have multiple valence bands[5] which contribute to the thermoelectric properties. However, unlike PbTe, SnTe is inherently riddled with defects which results in a heavily doped ($p \sim 10^{20}$–10^{21} cm^{-3}) material and a mediocre zT (around 0.5 at 900 K)[6, 7]. Nonetheless, several works have confirmed the existence of two valence bands (as in PbTe) and have estimated their transport parameters[6, 8-11].

SnTe has a large valence band offset, ΔE, of around 0.3-0.4 eV at room temperature—larger than PbTe which is closer to 0.1 eV (Figure 1c)[9, 12]. The two valence bands in SnTe are known to give rise to a unique Seebeck coefficient behavior as the carrier concentration is varied (Seebeck Pisarenko relation). A minimum Seebeck coefficient is observed in the Pisarenko plot (Fig 1a) near n=1-2×10^{20} cm^{-3}, followed by a maximum at about n=8×10^{20} cm^{-3}. Theoretical calculations confirm the position of the two valence bands in k-space and have provided some insight into their character[13-16]. Very recently Zhang et al reported an enhanced Seebeck coefficient in SnTe doped with In. A marked increase of zT with temperature and a maximum zT value of 1.1 were observed at 873 K[17], suggesting that SnTe may in fact be a promising thermoelectric material. Tan reported a high zT of 1.3 for Cd-doped SnTe with endotaxial CdS nanoscale precipitates[18]. Han and Chen et al reported zT of 0.9-1 for SnTe-$AgSbTe_2$ alloys[19, 20]. Other than thermoelectric properties, other works have discussed SnTe and its alloys as useful for long wavelength detectors[21-23], or most recently as topological insulators[14, 24, 25].

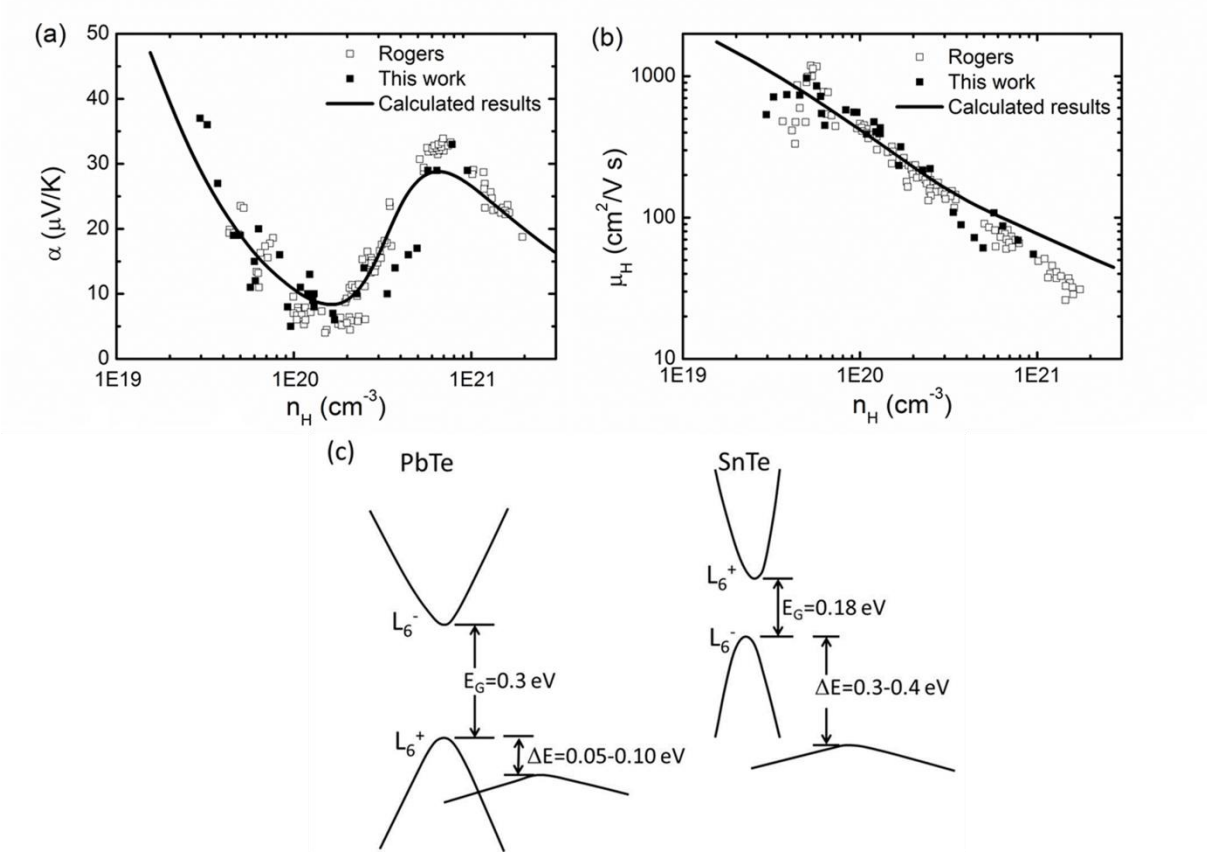

PCCP

RSCPublishing

ARTICLE

Figure 1. a) Seebeck coefficient and b) Hall mobility as a function of Hall carrier concentration at 300 K for $SnTe_{1-x}I_x$ and $SnTe_{1+y}$, $Gd_zSn_{1-z}Te$. Solid squares are our experimental results, open squares are Rogers' reported results[9], solid curves are calculated from a two band model. c) A schematic diagram of the near edge band structure in PbTe and SnTe. (Rogers et al reported a band offset of 0.3 eV for SnTe. Our results yielded different fitting parameters, and we found that 0.4 eV was required for best fit.)

The unique Seebeck coefficient behavior of SnTe as the carrier concentration stimulates our interests to explore the nature of electrical transport in SnTe and to optimize the thermoelectric properties. Finding the optimum doping level in semiconductors with complicated band structures is crucial to obtaining a thermoelectric material with the optimum performance. In this work, we will show that both the Seebeck coefficient and zT value increase either by substituting donor (I) or acceptor (extra Te and Gd) dopants. We observe that the peak zT value ($zT_{max,1}$=0.6 at 673 K) of I-doped SnTe with decreased carrier concentration (3×10^{19} cm^{-3}) is higher than the other peak zT value of extra Te or Gd-doped SnTe ($zT_{max,2}$=0.4 at 773 K) with increased carrier concentration (6×10^{20} cm^{-3}); suggesting that the light, primary valence band is most important in these systems. This unique behavior is contrary to the behavior in the lead chalcogenides where the second, heavy band usually leads to improved figure of merit.

2. Experimental

Polycrystalline samples of $SnTe_{1-x}I_x$ ($0\leq x\leq0.02$,), $SnTe_{1+y}$ ($0<y\leq0.015$), $Gd_zSn_{1-z}Te$ ($0<z\leq0.02$) were prepared by using a melt alloying and hot pressing technique. Pure elements and TeI_4 (Sn, 99.999%; Te, 99.999%; Gd, 99.99%; TeI_4, 99.999%, ultra dry) were weighed out according to each composition and loaded into quartz ampoules, which were then evacuated and sealed. The sealed ampoules were slowly heated to 1273 K and kept for 24 h followed by water quenching. The ingots obtained were further annealed at 973 K for 120 h before being crushed and ground into fine powders. The powders were then hot pressed at 823 K under 1 atm argon with 40 MPa pressure for 30 min. A typical disk shaped sample obtained is 12 mm in diameter with density no less than 95% of theoretical density (6.46 g/cm^3). The electrical resistivities and Hall coefficients (R_H) were measured by using the Van der Pauw method in a magnetic field up to ±2 T[26]. The Seebeck coefficients were obtained by measuring the thermoelectric voltages as well as temperatures with T-type thermocouples[27]. The thermal conductivities were obtained by $\kappa=C_p\lambda d$ with the thermal diffusivity λ measured by the laser flash method (Netzsch LFA 457), where d is the geometric density. The heat capacity C_p was determined by $C_p=C_{p,300}+C_{p1}\times((T/300)^{\alpha}-1)/((T/300)^{\alpha}+C_{p1}/C_{p,300})$[28], where T is the absolute temperature, $C_{p,300}$ is the specific heat capacity at 300 K. For SnTe, $C_{p,300}$ is 0.1973 J/g K, C_{p1} is 0.115 J/g K, α is 0.63[28]. All the test data were collected during both heating and cooling with both datasets shown.

Transport properties were modeled following previous work[29, 30]. The light and heavy valence band properties were calculated by evaluating the full generalized Fermi integrals as a function of chemical potential. The light band was assumed to be a nonparabolic, Kane band, with a nonparabolicity parameter, β, given by κ_BT/E_g where E_g was assumed constant at 0.18 eV [31], while the heavy band was modeled as a parabolic band. (More information about the specific modeling parameters can be found in the supplementary material.)

3. Results and Discussion

The measured Hall carrier concentration ($p_H=1/e\ R_H$) of $SnTe_{1-x}I_x$, $SnTe_{1+y}$ and $Gd_zSn_{1-z}Te$ samples at 300 K are shown in Figure 2a. The Hall carrier concentration of stoichiometric SnTe was found to be around $1.1\pm0.2\times10^{20}$ cm^{-3}at 300 K when prepared by using the described method. This value is slightly lower than Zhang's report (about 2×10^{20} cm^{-3})[17]. Extra Te is thought to induce cation vacancies which act as double acceptors[4, 32]. Brebrick, whose data is also shown in Figure 2, studied closely Te solubility in SnTe and concluded the phase width always leaned towards the Te rich side due to Sn vacancies that leads the heavily p-type character of intrinsic SnTe. Our work agrees with the cation vacancy mechanism and yields ~1.7 holes per Te atom, although, Brebrick saw more (3 holes per Te atom)[6]. Because Brebrick used carefully controlled and measured data for Te content while we use nominal composition only, Te loss through vaporization during synthesis is a plausible explanation of the difference. Dopant solubility in SnTe has been thoroughly studied by Rogacheva et al, they investigate the complexities involved with doping phases which are intrinsically nonstoichiometric[33]

Gd with normal valence Gd^{3+}might be expected to substitute for Sn^{2+} and be an electron donor, but instead Gd is observed to cause an increase in p-type, hole carrier concentration. Similar results were reported by Story et al who suggests Gd is a resonant dopant, no Seebeck increase was observed relative to Te-doped samples in this work which would indicate resonant states—probably due to a lower Gd content (<1%) and higher temperatures in comparison to the literature[34]. While the exact mechanism of Gd doping is not clear, the Gd-doped samples showed a linear increase in n_H with Gd doping for z>0.0025.

We also attempted to counter dope SnTe by substituting Te with Iodine. While much work has been done on cationic substitutions, far fewer works study how SnTe is affected by Iodine substitution. As pointed out by Rogacheva et al, the cationic dopants that have the highest solubility are those which have similar ionic radii to Sn. Hence, Iodine should be a good candidate for anionic substitutional doping in SnTe. As observed in Figure 2a, the carrier concentration linearly decreased to as low as 3×10^{19} cm^{-3} with ~40% doping efficiency assuming that one electron is donated per iodine atom. The doping efficiency appears linear until N_I ~ $25\times10^{19}cm^{-3}$ (x = 0.015) where the carrier concentration continues to decrease, but at a slower rate. The observed carrier concentration has been achieved by previous authors[35-37] , but

their interpretation of it and its significance to the thermoelectric properties was not thoroughly studied.

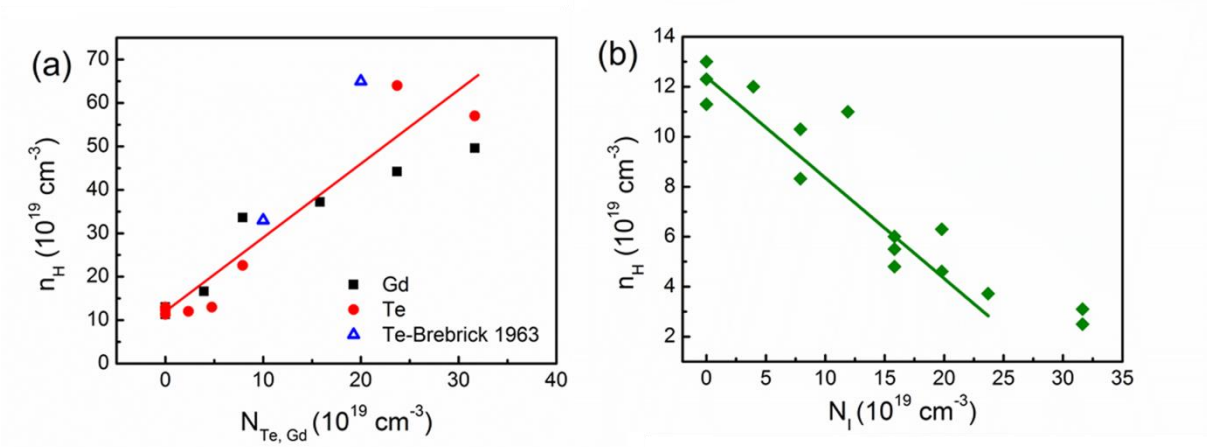

Figure 2. Hall carrier concentration as a function of dopant concentration a) Gd, Te excess as acceptors, b) I as donor. Solid lines represent guides to the eye for our data and correspond to 1.7 holes per atom for the Gd/excess Te case shown in a, and 0.4 electrons per Iodine atom as in b.

The measured temperature dependent transport data for samples with nominal composition $SnTe_{1-x}I_x$, $Gd_zSn_{1-z}Te$, and $SnTe_{1+y}$are shown in Figure 3. Stoichiometric SnTe data reported by Zhang et al (green dashed lines for samples with a slightly different n_H than SnTe in this work) are also shown. Degenerate semiconducting behavior, indicated by an increasing Seebeck coefficient and resistivity with temperature, is observed for all samples. As the iodine content is increased, the measured Seebeck coefficient and electrical resistivity increase, consistent with the decrease of Hall carrier concentrations shown in Figure2. This suggests that I atoms substitute for Te and supply extra electrons which compensate the effect of intrinsic Sn vacancies. Conversely, the p-type dopants (Gd and excess Te) reduce the resistivity consistent with an increase in carrier concentration. The Seebeck coefficient for these samples, unlike in the I doping case, show an increase with increasing doping level at room temperature—a direct consequence of the two band behavior described in Figure 1. Further, the most heavily doped sample (6×10^{20} cm^{-3}) also has nearly the highest Seebeck coefficient at room temperature, but it does not increase as much with temperature as samples with lower doping levels.

The total thermal conductivity and the calculated lattice thermal conductivity of $SnTe_{1-x}I_x$ samples are shown in Figure 3(e, f). The total thermal conductivity of the undoped SnTe decreases with temperature, reaching 2.3-3.0W/m K at 773K.The thermal conductivities of all the I-doped $SnTe_{1-x}I_x$ are lower than that of undoped SnTe, which comes from the reduction of electronic thermal conductivity as a result of a decreasing hole concentration. The lattice thermal conductivity, κ_L, is calculated by subtracting the electronic contribution ($\kappa_e = LT/\rho$) from the total thermal conductivity, where L is the Lorenz number that was estimated from a two-band model ($L=(L_L\sigma_L T+L_\Sigma\sigma_\Sigma T+\kappa_{bipolar})/(\sigma_L T+\sigma_\Sigma T)$, where $\kappa_{bipolar}=T(\sigma_1\alpha_1^2+\sigma_2\alpha_2^2-(\sigma_1\alpha_1+\sigma_2\alpha_2)^2/(\sigma_1+\sigma_2))$). The lattice thermal conductivity of all the I-doped $SnTe_{1-x}I_x$ samples decreased with temperature, and then increased when the temperature is over 600 K. This suggests that bipolar effects occur in I-doped $SnTe_{1-x}I_x$ samples with lower carrier concentrations at high temperature. κ_L is not shown for Te and Gd doped samples, which were shown to be additionally complex due to large contributions from the Σ band; instead the estimates are included in the supplementary material (Figure S3).

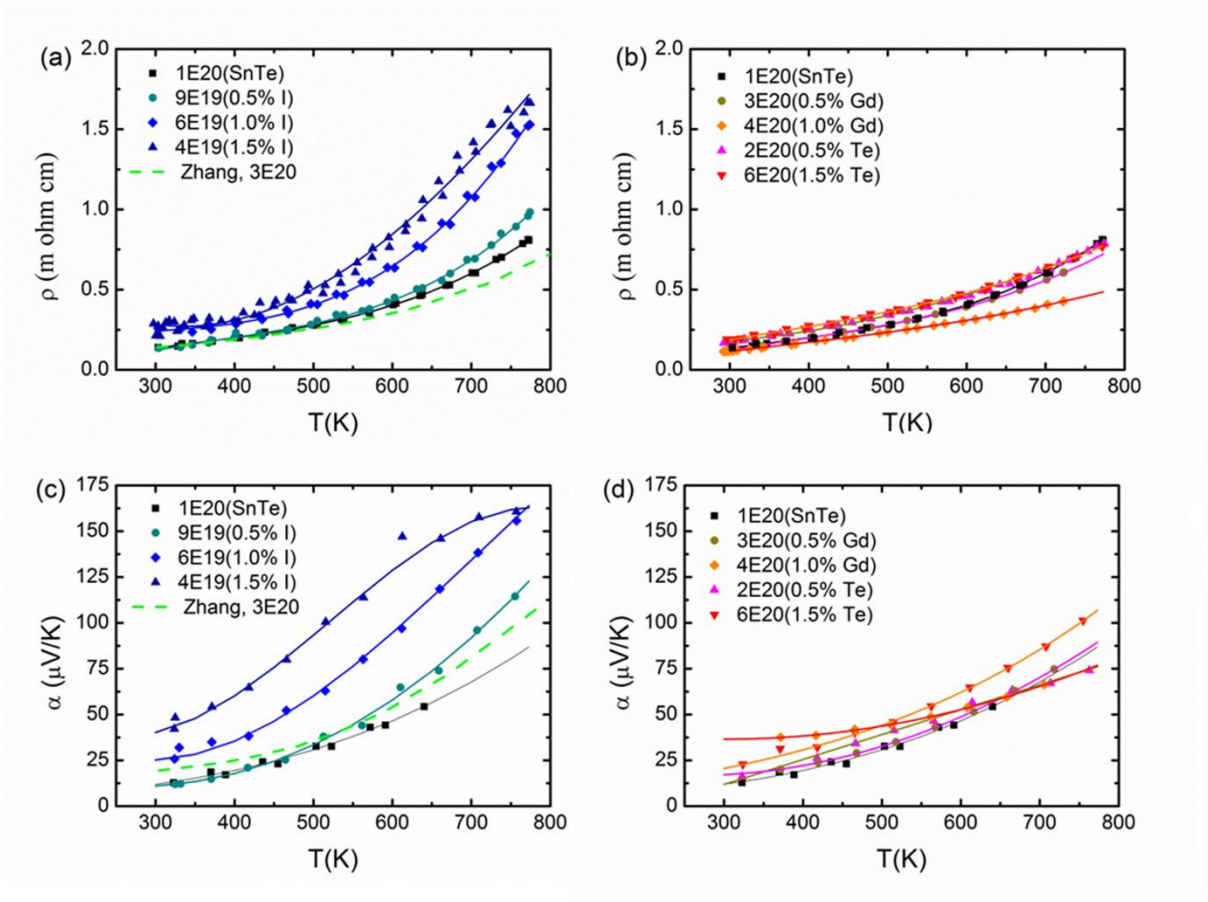

Figure 3.Thermoelectric transport properties for various SnTe samples: a) resistivity of SnTe and $SnTe_{1-x}I_x$, b) resistivity of SnTe, $SnTe_{1+y}$ and $Gd_zSn_{1-z}Te$, c) Seebeck of SnTe and $SnTe_{1-x}I_x$, d) Seebeck of SnTe, $SnTe_{1+y}$ and $Gd_zSn_{1-z}Te$, e) thermal conductivity and lattice thermal conductivity of SnTe and $SnTe_{1-x}I_x$, f) thermal conductivity and lattice thermal conductivity of SnTe, $SnTe_{1+y}$ and $Gd_zSn_{1-z}Te$. Legends indicate room temperature Hall carrier concentrations and a brief description of the samples as follows: $SnTe_{1-x}I_x$, $Sn_{1-x}Gd_xTe$, and $SnTe_{1+x}$ for Iodine doped (a,c,e), Gd doped (b, d, f), and excess Te (b, d, f) samples respectively. All plots show both raw experimental data (points) and polynomial fits (lines).

Full optimization of SnTe yields a higher *zT* (average and peak) for samples doped with Iodine. The thermoelectric figure of merit, *zT*, is shown as a function of temperature in Figure 4 for Iodine, Gd, and Te rich samples along with results from Zhang et al for an undoped and an In doped sample[17]. We show that the undoped SnTe (n_H = 1.1×10^{20} cm^{-3}) shows low *zT* values over the measured temperature range yielding a maximum of 0.23 at 773 K. This is lower than the reported *zT* value (0.39) of SnTe with a higher carrier concentration (n_H = 2×10^{20} cm^{-3}) at the same temperature from Zhang et al (as shown in Figure 4a). From Figure 4a, *zT* values increased with donor I-dopant and a peak *zT* value of 0.6 was obtained for $SnTe_{0.985}I_{0.015}$ at 700 K, corresponding to an optimum doping level of around 4×10^{19} cm^{-3}, which was the lowest attainable with iodine doping that did not lead to hysteretic behavior in the transport properties (see supplementary material Figure

S5a). zT values of 0.45-0.6 were obtained for several samples with room temperature n_H of 4.0-6.1×10^{19} cm^{-3}. This means that decreasing carrier concentration is a valid approach to optimize zT of SnTe by doping with iodine.

Alternatively, zT values increased with acceptor Te or Gd-dopant also. The other peak zT value of 0.4 was obtained for the most heavily doped samples ($Gd_{0.01}Sn_{0.99}Te$ and $SnTe_{1.015}$, n_H = 4-6×10^{20} cm^{-3}) at 773K—about 30% lower than the iodine doped samples. Unlike conventional single band behavior, we show that both I-doped SnTe and Gd-doped SnTe have higher zT values than that of stoichiometric SnTe. Figure 4c shows the average zT value ($\overline{zT} = \frac{\int_{300}^{773} zTdT}{773-300}$) of I-doped and Te-rich SnTe samples along with Zhang et al $In_{0.0025}Sn_{0.9975}Te$ samples over the temperature range of 300-773 K. $SnTe_{1.015}$ shows an average zT of 0.15, but the average zT value of best I-doped SnTe (0.35) is about the same as the best In-doped sample (0.32) which contains resonant states. We believe that carrier concentration optimization will prove useful for zT enhancement in SnTe in the moderate temperature regime, without resonant impurities.

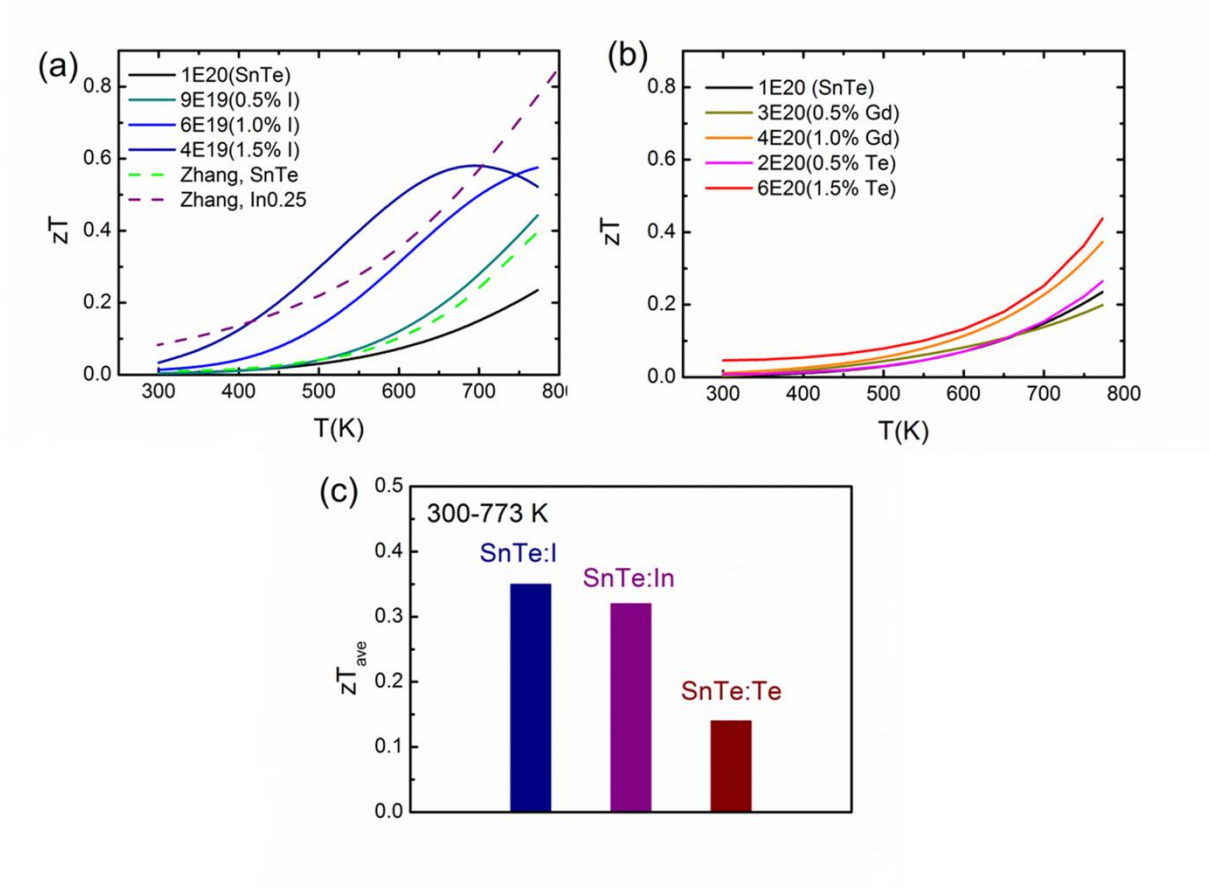

Figure 4. a) zT of $SnTe_{1-x}I_x$ as function of temperature, data (dashed lines) are from the literature [17]. b) zT of $SnTe_{1+y}$ and $Gd_zSn_{1-z}Te$ as function of temperature. c) the average zT between 300 and 773 K for optimum doped samples, data of SnTe:In are from the literature[17]. zT estimates are obtained from polynomial fits of transport data in Figure 3.

The Seebeck coefficient as a function of Hall carrier concentration (Pisarenko plot) is shown in Figure 1a for $SnTe_{1-x}I_x$ and $SnTe_{1+y}$, $Gd_zSn_{1-z}Te$ at 300 K along with reported results from Brebrick and Rogers et al [6, 9]. The plot shows a unique, non-monotonic n_H dependence brought about by the two interacting valence bands. For carrier concentration of 1-2×10^{20} cm^{-3}, the Seebeck coefficient shows a minimum value of about 5-10 μV/K. The Seebeck coefficient then increases to a maximum of about 30 μV/K at carrier concentration of 6-8×10^{20} cm^{-3}. Figure 1b shows the relationship between the carrier mobility and Hall carrier concentration of all the samples as well as data reported by Rogers et al. at 300 K[9]. The carrier mobility of stoichiometric SnTe is about 400-500 cm^2/V-s at room temperature and always decreases with increasing carrier concentration for all $SnTe_{1-x}I_x$ and $SnTe_{1+y}$, $Gd_zSn_{1-z}Te$ samples. The experimental data of both Seebeck coefficient and mobility are fitted by a two band model (the solid curve) using a Kane band (SKB) for the light and a parabolic band (SPB) for the heavy valence band (as described in detail in the supplementary material). As shown in Figure 5, the high temperature Seebeck coefficient and carrier mobility could also be explained by the same model, with the valence band offset (ΔE) and band effective masses allowed to change as fitting parameters as a function of temperature. The non-monotonic behavior for the Seebeck coefficient becomes less significant at high temperature (Figure 5a), probably a result of a broadening Fermi distribution and temperature dependent shifts in the band structure. By fitting experimental results we determine that the density of states effective mass m_L^* of the light valence band is 0.14 m_e for $SnTe_{1-x}I_x$ at 300 K, and it changes with temperature roughly according to $dlnm_L^*/dlnT$=0.55. Similar temperature dependence has been

reported in other IV-VI compounds with similar band structure[1, 29, 38]. Little is known about the parameters for the heavy band, and they are difficult to determine directly using experimental techniques. As a result, they were adjusted to fit the experimental Seebeck and mobility data. The density of states effective mass m_H^* was fit to be 1.7 m_e at 300 K, and it changes with temperature according to $dlnm_H^*/dlnT=0.5$. The 300K values are comparable to those reported by Brebrick et al. [6]. The valence band offset energy, ΔE, between the two bands was found to be 0.4 eV at 300 K according to the fitting result and decreases roughly linearly with temperature at a rate of 3.4×10^{-4} eV/K.

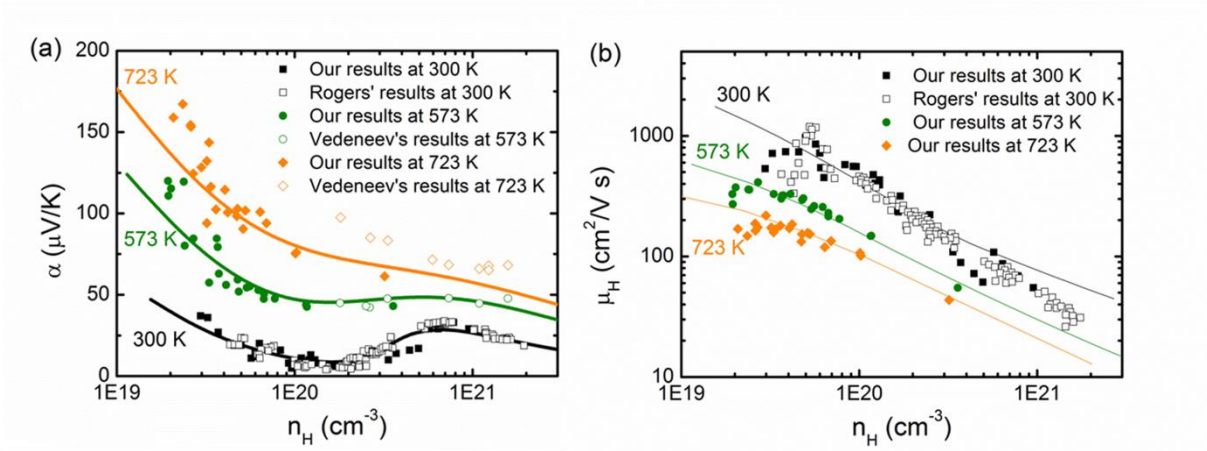

Figure 5 a) Seebeck coefficient and b) Hall mobility as a function of Hall carrier concentration at different temperatures. Solid symbols represent our experimental results, open symbols correspond to literature data (Vendeev[7] and Rogers[9]). Each is presented at three temperatures: 300, 573, and 723 K which are given by squares, circles, and diamonds respectively. Solid curves represent the results of the two band model.

Figure 6 shows zT as a function of Hall carrier concentration for $SnTe_{1-x}I_x$, $SnTe_{1+y}$and $Gd_zSn_{1-z}Te$ samples. Note that a local minimum exists in zT vs. n_H for temperatures of 300 and 600 K, which correspond to a carrier density of $\sim1\times10^{20}$ cm^{-3}—approximately the composition of stoichiometric SnTe. At a higher temperature of 773 K, the model predicts a single maximum in zT as seen in most thermoelectric materials, but the peak is broadened due to the increasing influence of the second band. From Figure 6, both the experimental and model results indicate a significant zT increase with decreasing carrier concentration, yielding a maximum in the 10^{18} – 10^{19} cm^{-3} range. In this work, the solubility of I in $SnTe_{1-x}I_x$ (x = 0.015, $n_H\sim4\times10^{19}$ cm^{-3}) has limited us from achieving the optimized n_H for the predicted maximum zT to be obtained (which requires $n_H\sim8\times10^{18}$ cm^{-3}). While we do expect bipolar effects to begin to play a role at low doping levels, which is not accounted for in this model, the conclusions remains that optimizing SnTe carrier concentration towards the light band results in significant improvement.

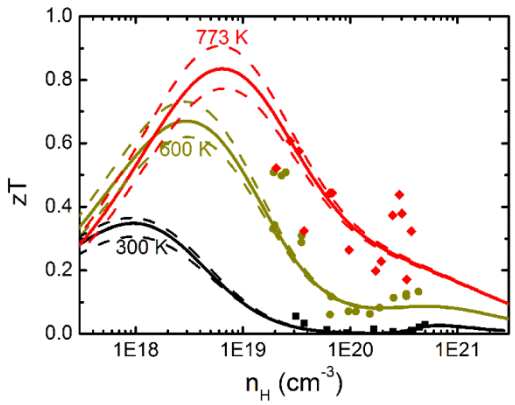

Figure 6 zT as a function of Hall carrier concentration for $SnTe_{1-x}I_x$ and $SnTe_{1+y}$, $Gd_zSn_{1-z}Te$. Solid curves are modeling results, dashed lines are uncertainty values for the model zT which account for a $\pm10\%$ error in κ_L. The calculated lattice thermal conductivity of 2.5±10% W/m K (300 K), 1.23±10% W/m K (600K) and 1.0±10% W/m K (773 K) were used in the zT calculation as obtained from I-doped samples (Figure 3e).

While both SnTe and PbTe are IV-VI materials have the same crystal structure and similar electronic band structures, their thermoelectric performance and optimization strategies are quite different. At first, one might write off SnTe due to its large intrinsic defect concentration and higher lattice thermal conductivity when compared to PbTe. However, this work suggests that it does in fact give a reasonable zT when optimizing towards the low carrier concentration, light band over the poorer heavy band; this is achieved by doping with iodine. While valley degeneracy and band convergence play a crucial role in the high zT for PbTe (more than 1.5 at T ~ 800 K), the larger band offset in SnTe (0.3 eV for SnTe vs 0.1 eV for PbTe at 300 K) makes convergence unattainable in SnTe for temperatures below its melting point. In addition, the thermoelectric quality factor[29, 39] $B=2\kappa_B^2\hbar C_l N_v/3\pi m_i^* E_{def}^2\kappa_L$ can be used to determine the quality for the light and heavy band to be 0.42 and 0.27 respectively in SnTe at 600 K. The light band is estimated to have nearly 50% higher quality factor than the heavy band in this system due primarily to the low band mass (and corresponding high mobility). Coupled with a large band offset (~6 k_BT at 600 K), the peak zT for SnTe occurs for a chemical potential near to the light valence band edge. This is in contrast to PbTe where the heavy band is believed to have as good or better quality factor than the light band with a much smaller band offset ($\Delta E\sim1.5$ k_BT at 600 K)[39]. So, while valley degeneracy and the heavy band at Σ play an important role in PbTe[1], they are not viable options for improving zT in SnTe.

4. Conclusions

While undoped SnTe has very poor thermoelectric performance, SnTe can be greatly improved through carrier density tuning. We have shown that by either increasing or decreasing the carrier concentration, the zT can be improved relative to naturally synthesized, nominally undoped SnTe. A peak zT value of 0.6 is obtained for $SnTe_{0.985}I_{0.015}$ sample with a lower carrier concentration of 4×10^{19} cm^{-3}, which is about 50% higher than the other peak zT value of 0.4 for $SnTe_{1.015}$ with a higher carrier concentration of $p_H = 6\times10^{20}$ cm^{-3}. Transport property models predict higher zT if the carrier concentration could be reduced further to 1×10^{19} cm^{-3}. Different from In-doped SnTe that alters the host band structure, this work revealed the inherent merit of SnTe thermoelectric materials. It is worth noting that an average zT of 0.35 was obtained for light band dominated $SnTe_{0.985}I_{0.015}$ (300-773 K); this is nearly the same as In-doped SnTe (0.32) with resonant states averaged over the same temperature range. With further band engineering SnTe may become an efficient lead free alternative of lead chalcogenide thermoelectric materials.

Acknowledgements

The authors would like to acknowledge funding from the ITMO University in Saint Petersburg Russia. GJS and ZMG would like to acknowledge funding from The Materials Project, which is supported by Department of Energy's Basic Energy Sciences program under Grant No. EDCBEE, DOE Contract DE-AC02-05CH11231.

References

1. Y. Pei, X. Shi, A. LaLonde, H. Wang, L. Chen and G. J. Snyder, *Nature*, 2011, **473**, 66-69.
2. H. Wang, Y. Pei, A. D. LaLonde and G. J. Snyder, *Advanced materials*, 2011, **23**, 1366-1370.
3. K. F. Hsu, S. Loo, F. Guo, W. Chen, J. S. Dyck, C. Uher, T. Hogan, E. Polychroniadis and M. G. Kanatzidis, *Science*, 2004, **303**, 818-821.
4. I. U. r. I. Ravich, B. A. e. Efimova and I. A. Smirnov, *Semiconducting lead chalcogenides*, Plenum Publishing Corporation, 1970.
5. F. HERMAN, R. KORTUM, L., I. ORTENBURGER, B. and J. P. VAN DYKE, *J. Phys. Colloques*, 1968, **29**, C4-62-C64-77.
6. R. F. Brebrick and A. J. Strauss, *Physical Review*, 1963, **131**, 104-&.
7. V. P. Vedeneev, S. P. Krivoruchko and E. P. Sabo, *Semiconductors*, 1998, **32**, 241-244.
8. R. L. Bernick and L. Kleinman, *Solid State Communications*, 1970, **8**, 569-&.
9. L. M. Rogers, *Journal of Physics D-Applied Physics*, 1968, **1**, 845-&.
10. S. Santhanam and A. Chaudhuri, *Materials Research Bulletin*, 1981, **16**, 911-917.
11. P. Gonzalez, J. Agapito and D. Pardo, *Journal of Physics C: Solid State Physics*, 1986, **19**, 899.
12. A. N. Veis and Y. I. Ukhanov, *Sov Phys Semicond+*, 1976, **10**, 780-783.
13. D. J. Singh, *Funct Mater Lett*, 2010, **3**, 223-226.
14. T. H. Hsieh, H. Lin, J. W. Liu, W. H. Duan, A. Bansil and L. Fu, *Nat Commun*, 2012, **3**.
15. A. Jain, S. P. Ong, G. Hautier, W. Chen, W. D. Richards, S. Dacek, S. Cholia, D. Gunter, D. Skinner, G. Ceder and K. A. Persson, *APL Materials*, 2013, **1**, -.
16. K. M. Rabe and J. D. Joannopoulos, *Phys Rev B*, 1985, **32**, 2302-2314.
17. Q. Zhang, B. L. Liao, Y. C. Lan, K. Lukas, W. S. Liu, K. Esfarjani, C. Opeil, D. Broido, G. Chen and Z. F. Ren, *Proceedings of the National Academy of Sciences of the United States of America*, 2013, **110**, 13261-13266.
18. G. Tan, L.-D. Zhao, F. Shi, J. W. Doak, S.-H. Lo, H. Sun, C. Wolverton, V. P. Dravid, C. Uher and M. G. Kanatzidis, *Journal of the American Chemical Society*, 2014.
19. Y. Chen, M. D. Nielsen, Y.-B. Gao, T.-J. Zhu, X. Zhao and J. P. Heremans, *Advanced Energy Materials*, 2012, **2**, 58-62.
20. M. K. Han, J. Androulakis, S. J. Kim and M. G. Kanatzidis, *Advanced Energy Materials*, 2012, **2**, 157-161.
21. D. Khokhlov, L. Ryabova, A. Nicorici, V. Shklover, S. Ganichev, S. Danilov and V. Bel'kov, *Appl Phys Lett*, 2008, **93**, -.
22. D. R. Khokhlov, I. I. Ivanchik, S. N. Raines, D. M. Watson and J. L. Pipher, *Appl Phys Lett*, 2000, **76**, 2835-2837.
23. J. V. Gumenjuk-Sichevskaya and F. F. Sizov, *Semicond Sci Tech*, 1999, **14**, 1124-1131.
24. S. Y. Xu, C. Liu, N. Alidoust, M. Neupane, D. Qian, I. Belopolski, J. D. Denlinger, Y. J. Wang, H. Lin, L. A. Wray, G. Landolt, B. Slomski, J. H. Dil, A. Marcinkova, E. Morosan, Q. Gibson, R. Sankar, F. C. Chou, R. J. Cava, A. Bansil and M. Z. Hasan, *Nat Commun*, 2012, **3**.
25. M. Safdar, Q. S. Wang, M. Mirza, Z. X. Wang, K. Xu and J. He, *Nano Lett*, 2013, **13**, 5344-5349.
26. K. A. Borup, E. S. Toberer, L. D. Zoltan, G. Nakatsukasa, M. Errico, J.-P. Fleurial, B. B. Iversen and G. J. Snyder, *Review of Scientific Instruments*, 2012, **83**, 123902.
27. S. Iwanaga, E. S. Toberer, A. LaLonde and G. J. Snyder, *Review of Scientific Instruments*, 2011, **82**, 063905.
28. M. Wagner, *These de doctorat, Universität Wien*, 2007.
29. H. Wang, Y. Z. Pei, A. D. LaLonde and G. J. Snyder, *Proceedings of the National Academy of Sciences of the United States of America*, 2012, **109**, 9705-9709.
30. D. M. Rowe, *CRC Handbook of Thermoelectrics*, Taylor & Francis, 2010.
31. L. M. Rogers, *British Journal of Applied Physics*,

1967, **18**, 1227-&.
32. R. F. Brebrick, *J Phys Chem Solids*, 1963, **24**, 27-&.
33. E. Rogacheva and O. Nashchekina, *physica status solidi (a)*, 2006, **203**, 2856-2860.
34. T. Story, M. Gorska, A. Lusakowski, M. Arciszewska, W. Dobrowolski, E. Grodzicka, Z. Golacki and R. Galazka, *Physical review letters*, 1996, **77**, 3447-3450.
35. E. Trifonova and L. Karagiozov, *Crystal Research and Technology*, 1983, **18**, 315-320.
36. M. Moldovanova, E. Trifonova, R. Assenov and L. Karagiozov, *physica status solidi (a)*, 1980, **58**, K47-K50.
37. R. Assenov, V. Moshnikov and D. Yaskov, *physica status solidi (a)*, 1985, **88**, K27-K30.
38. H. Wang, E. Schechtel, Y. Pei and G. J. Snyder, *Advanced Energy Materials*, 2013, **3**, 488-495.
39. Y. Pei, H. Wang and G. J. Snyder, *Adv Mater*, 2012, **24**, 6125-6135.